ARTICLE

Pressure Measurement Based on a Multimode Phase Retarder Plastic Optical Fiber

Rei A. Furukawa,*,† Akihiro Tagaya,‡ and Yasuhiro Koike†

Faculty of Science and Technology, Keio University, 3-14-1 Hiyoshi, Kohoku-ku, Yokohama 223-8522, Japan, and Koike Photonics Polymer Project, ERATO-SORST, Japan Science and Technology Agency, Shinkawasaki Town Campus Building E, 7-1 Shinkawasaki, Kawasaki 212-0032, Japan

ABSTRACT This paper demonstrates a polarimetric pressure measurement using a multimode phase retarder plastic optical fiber fabricated from a birefringence-controllable copolymer. An optimal composition that gives the most pronounced response to pressure was studied by comparing the extinction ratio of fibers fabricated with different copolymer compositions. A simple sensor design with a single-fiber structure was proposed that has detection capabilities similar to those of the conventional dual-path structure of a Mach−Zehnder interferometer. A linear relationship between the fiber birefringence and the applied pressure was observed in a range from 0 to 0.06 MPa. A polarimetric sensitivity of 1.56×10^{-5} MPa^{-1} was obtained experimentally from the relationship between the birefringence and pressure.

KEYWORDS: copolymer • phase retarder • multimode optical fiber • pressure sensing • birefringence • polarimetry

INTRODUCTION

Various types of fiber-optic pressure sensors have been developed because of advantages such as a lack of interference from electric or magnetic fields and high sensitivity, among others (1−9). A sensor type that uses Mach−Zehnder interferometry is capable of highly sensitive pressure detection and is often used as a hydrophone (10−13). However, despite of the high sensitivity, such sensors have complicated structures. Typically, the fiber used in this sensor type is a single-mode fiber (SMF) of polarization-maintaining (PM) type such as an elliptical core, a bow tie, a side hole, and a photonic crystal fiber (14). Despite their smooth output wavefront that enables accurate phase detection, two or more ray paths are necessary in order to quantify the phase shift in a detectable form. In other words, interference between the functioning and reference paths is their detection mechanism.

This paper demonstrates a preliminary design of a fiber-optic pressure sensor using a copolymer-based phase retarder plastic optical fiber (POF). Like many other reported models of POF sensors (15−18), the proposed sensor, in which the core diameter of the phase retarder POF is extremely large (667 μm), has the advantage of light-coupling robustness compared to sensors using glass-based SMFs (19). Furthermore, the proposed pressure sensor is unique also from the design aspect: no other types of optical fibers except for phase retarder POFs can accomplish pressure detection with the proposed sensor structure. Despite of the detection principle being similar to the Mach−Zehnder type, the proposed sensor requires only one fiber for pressure detection, because the modes corresponding to the fast and slow optical axes coexisting in one fiber can replace the function of two PM-SMFs of the conventional sensor models. In this way, the phase difference between two groups of modes interferes with a particular polarization state at the output, so the phase shift is detectable only by placement of a polarizer before the power detector. Thus, the pressure-sensing part is one portion of the fiber itself, unlike the known design that uses another birefringent crystal (1).

The phase retarder POF is fabricated using the two monomer species methyl methacrylate (MMA) and benzyl methacrylate (BzMA). In our former publications, these materials were shown to be uniquely suitable for fabricating a multimode fiber with a high-polarization-maintaining property (19−21), whereas the propagation in conventional POFs is known to disturb the initial linear polarization state to some extent (22). MMA and BzMA are known to have opposite birefringence properties for both types of birefringence that coexist in the polymeric material, namely, orientational and photoelastic birefringence (23). Orientational birefringence is known to be related to the processing of the plastic above the glass-transition temperature, leading to the alignment of the polymer chain in a particular direction and thus creating optical anisotropy. The sign of the orientational birefringence is defined by whether $n_{\parallel} - n_{\perp}$ is positive or negative, where $n_{\parallel}$ and $n_{\perp}$ are the refractive indices of the axes parallel and perpendicular to the drawing direction, respectively. MMA and BzMA have negative and positive orientational birefringence, respectively. Photoelastic birefringence is understood to be related to a molecular movement as a result of the stress, which disappears once the stress is removed. The sign of this birefringence type is determined by whether the birefringence is positive or negative with regard to the applied pressure vector. The sign

* E-mail: fururei@a5.keio.jp.
Received for review December 3, 2008 and accepted February 16, 2009
† Keio University.
‡ ERATO-SORST, Japan Science and Technology Agency.
DOI: 10.1021/am800212y

Published on Web 03/09/2009

Table 1. Core Composition of the Test Copolymer Fibers (before Polymerization)

fiber name	MMA/BzMA composition (wt %)
fiber 1	77:23
fiber 2	82:18
fiber 3	87:13

relationship of MMA/BzMA photoelastic birefringence is also negative/positive. Hence, the copolymer pair of MMA and BzMA was formerly reported in its capability to eliminate both types of birefringence (23). However, the optimum composition for eliminating one type of birefringence is not necessarily the optimum composition for eliminating the other type of birefringence.

In this paper, we fabricated three P(MMA/BzMA) fibers with the purpose of obtaining the optimum composition that provides a minimal effect of orientational birefringence while having an active response in terms of photoelastic birefringence. In the absence of orientational birefringence, a P(MMA/BzMA) fiber acts as a PM fiber (21). On the other hand, when a plane-symmetrical stress such as macrobending along a plane is applied to the same fiber, the fiber no longer maintains the initial polarization state because of photoelastic birefringence (19). In this case, a phase shift is observed in the output light, which means that the P(MMA/BzMA) fiber exhibits clearly defined optical axes when it is under a plane-symmetrical pressure. Using this property, a preliminary design of a fiber-optic pressure sensor using the composition-optimized P(MMA/BzMA) fiber is demonstrated, followed by a discussion of its polarimetric sensitivity and dynamic range in the latter part of this article.

FABRICATION OF A PHASE RETARDER POF

Optimization of Copolymer Composition Using Refractive Index and Extinction Ratio (ER) Measurement. Three copolymer optical fibers were fabricated using the same method as that described in our former publication (19) except for variations in their copolymer composition. PMMA tubes with a closed end (inner/outer diameter = 14.7/22.0 mm; length = 600 mm) were fabricated in advance as the cladding part of the fiber preforms. For the core part, a solution of MMA and BzMA was placed in the center cavity of each PMMA tube and polymerized by heating. Three test fibers were fabricated with the compositions as shown in Table 1. The resulting preforms were heat-drawn in a furnace with a constant tension and draw ratio. Preforms were drawn to a diameter of core/fiber = 667/1000 μm.

The refractive index profiles of fibers 1−3 at the sodium D line (589 nm) were measured by the transverse interferometric technique using an interference microscope (Interphako; Carl Zeiss) (24). A standard plot of the P(MMA/BzMA) composition versus refractive index (at sodium D line) was obtained by measuring the refractive indices of copolymers with different compositions using a prism coupler (model 2010; Metricon Corp.). The standard plot was obtained for the purpose of comparing the fiber index profiles with the optimum values for eliminating orientational and photoelastic birefringence. The optimum values were adopted from Tagaya et al. (23). Tagaya et al. had derived these values by performing birefringence measurements based on optical heterodyne detection using films fabricated in various compositions (23).

Next, the ER response to applied pressure was measured for fibers 1−3 in order to characterize the polarization state change behavior. As shown in Figure 2, 1 m test fibers were used with the central 0.4 m subjected to pressure application. Acrylic boards were used for both the top and bottom plates, so that the two substrates have similar stiffness and pressure values from the top and bottom. At the sides of the test fiber, two additional copolymer fibers with the same diameter (1000 μm) were placed for stabilizing purposes, in order to uniformly apply the pressure from the plates. Precision weights were placed in sequence on the top plate. The total of the pressure applied to the fiber, P (Pa), was calculated using the following equation.

$$P = Wg/(3L)a \tag{1}$$

where each of the parameters has the following meanings: W (kg) = applied weight, g (m/s^2) = gravitational acceleration, L (m) = fiber and stabilizer length involved, and a (m) = fiber diameter. Here, g, L, and a are constant values, which are 9.8, 0.4, and 1.0×10^{-3}, respectively. P, L, and a are illustrated in Figure 2.

A 633-nm-output He−Ne laser was applied because its wavelength is acceptably close to the transmission window of the P(MMA/BzMA) POF (20) and it shows sufficiently high output power. The transmitting axis of the polarizer was fixed in a $\theta_{pol} = 45°$ configuration, where θ_{pol} is the angle between the polarizer axis and the pressure vector. The pinhole was in physical contact with the fiber end and positioned at the fiber core center in order to launch dominant modes while avoiding cladding modes. The output light from the test fiber was aligned to pass through an analyzer and was then detected by a power meter. The power was plotted at intervals of 10° of the analyzer angle (θ_A). An intensity curve was obtained over a total of 180° rotation of θ_A.

Properties of the Test Fibers. Refractive index profiles of fibers 1−3 are shown in Figure 1a. The refractive indices of compositions with eliminated orientational (MMA:BzMA = 82:18) and photoelastic (92:8) birefringence are obtained from the standard plot shown in Figure 1b and marked correspondingly in Figure 1a with broken lines.

As a result, fiber 2 has its dominant core region (from the center to around 0.7 of the core radius), which matched well with the zero-orientational birefringence index. The composition of fiber 2 is considered to be the optimum for a phase retarder fiber that should respond to pressure in a regular manner, because it is expected to show pressure-induced photoelastic birefringence of a certain magnitude while being insignificantly affected by

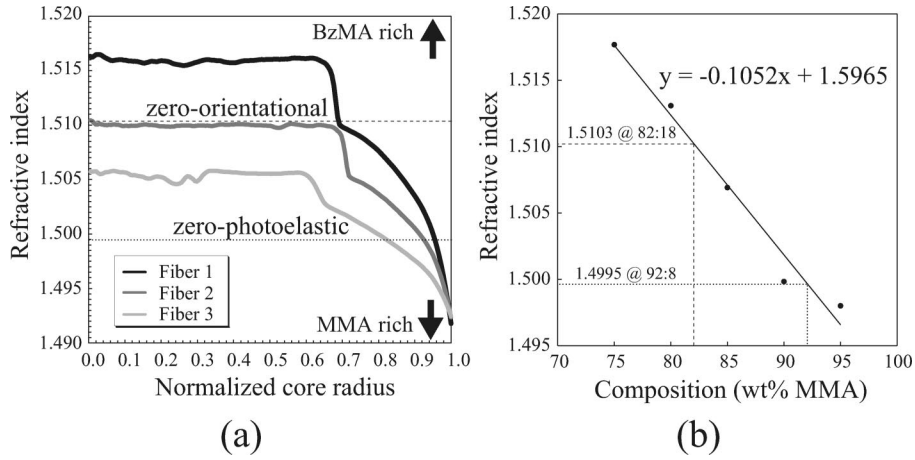

FIGURE 1. (a) Measured refractive index profiles of the test fiber cores. (b) Standard plot of the refractive index versus copolymer composition. Refractive indices of compositions for zero-orientational (MMA:BzMA = 82:18) and zero-photoelastic (92:8) birefringence are obtained from part b and are marked in part a with broken lines.

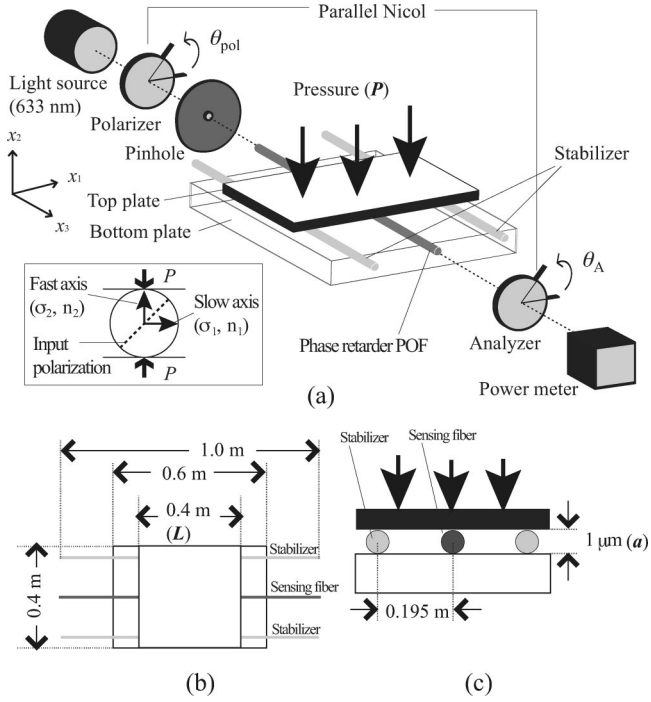

FIGURE 2. (a) Diagram of the pressure measurement setup using the phase retarder POF. The angle relationships of pressure vector *P*, the input polarization, and the fast/slow axes are shown schematically. (b) x_1−x_3 view. (c) x_1−x_2 view. Pressure is applied in the $-x_2$direction. Parallel Nicol is aligned diagonally to the pressure vector.

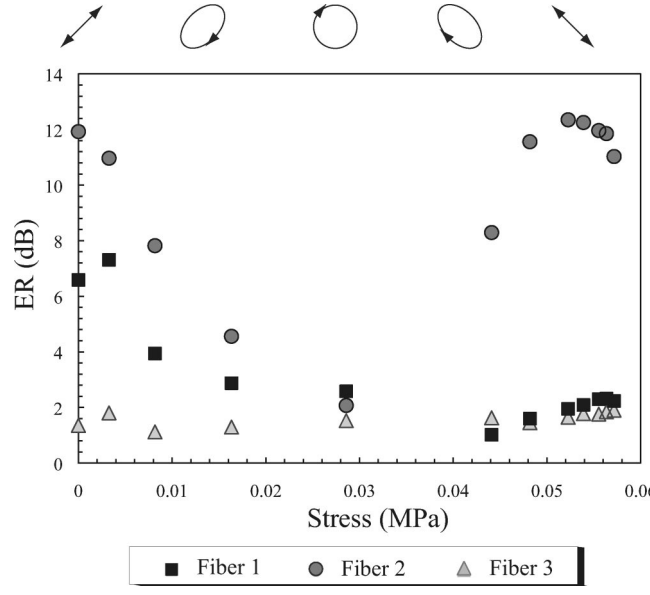

FIGURE 3. ER versus pressure plot of fibers 1−3. The change in the state of polarization of fiber 2 is shown in the top.

orientational birefringence. The other two fibers have compositions matching neither the zero-orientational birefringence nor the zero-photoelastic birefringence. These fibers are not expected to respond to pressure in a regular manner. This is because the phase change occurring during light propagation along the fiber will be more complicated if the two types of birefringences are both affected in a similar magnitude.

Figure 3 shows the ER shifts upon pressure application. The results suggest that fiber 2 provides a regular change in the polarization state when responding to the pressure. This behavior suggests a phase shifting as described in the upper part of the figure. The other two fibers do not show such periodic shifting of the ER values. Therefore, also the ER measurements support the assumption that fiber 2 has the most favorable property as a phase retarder POF for pressure-sensing purposes.

SENSOR DESIGN AND FABRICATION

The pressure measurement was carried out using the same setup as the one used for the ER measurement. Polarizers in the parallel Nicol configuration that were oriented diagonally referring to the pressure vector ($\theta_{pol} = \theta_A = 45°$) were placed on the input and output of the phase retarder POF (fiber 2). The angle of the parallel Nicol was fixed during the measurement. The intensity was monitored while changing the pressure.

The sensor mechanism is as described below. A phase change is induced by the photoelastic birefringence that is defined by

$$\text{photoelastic birefringence} = c\Delta\sigma \quad (2)$$

$$\Delta\sigma \propto P \quad (3)$$

where $\Delta\sigma$ is the difference in principle stress ($\sigma_1 - \sigma_2$ in Figure 2a; $\sigma_1 > \sigma_2$) and c is the photoelastic coefficient (23). The fast and slow axes of the phase retarder POF are decided from the relationship of the refractive index profile to the copolymer composition, which is shown in Figure 1a. The central flat part of the refractive index profile of the phase retarder POF (fiber 2) lies above the zero-photoelastic line, which means that it is off-balance toward the BzMA-rich side. The sign relationships of the photoelastic birefringence of PMMA and PBzMA are negative ($c < 0$) and positive ($c > 0$), respectively (23). Therefore, the refractive index profile of the phase retarder POF suggests that the fiber responds in a positive manner to the applied stress. The polarization state of the fiber output, which represents the phase difference generated during the propagation, was determined using the second polarizer and the power detector.

PERFORMANCE

Polarimetric Sensitivity. The intensity observed for the pressure measurement range from 0.00 to 0.06 MPa is shown in Figure 4. In addition to the data obtained in the original parallel Nicol configuration, which is in a diagonal orientation to the pressure vector ($\theta_{pol} = \theta_A = 45°$), data measured in 0 and 90° configurations were collected as well. As a result, the intensity curves obtained in 0 and 90° configurations are practically flat, while a clear cosine curve is observed in the original configuration.

The corresponding numerical data of the 45° configuration are listed in Table 2. The phase shift δ at each measurement point is obtained in relation to $\delta = \pi$, which is estimated from the minimum of the response curve shown in Figure 4. The birefringence B is calculated from eq 4 using the values $\lambda = 633.3$ nm and $L = 0.4$ m. δ and B are listed in Table 2.

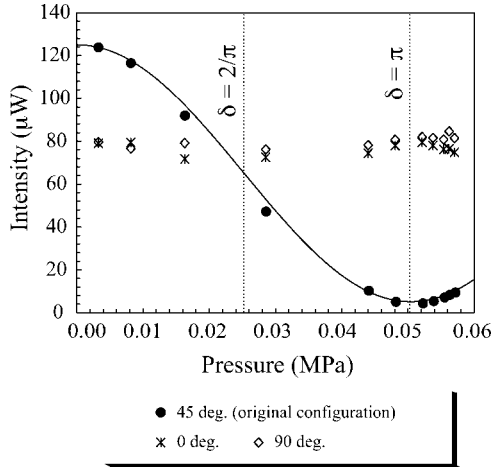

FIGURE 4. Power response to the applied pressure from 0.00 to 0.06 MPa. $\lambda = 633.3$ nm is used.

$$B = \frac{\delta\lambda}{2L} \quad (4)$$

A plot of the pressure versus birefringence is shown in Figure 5. The polarimetric sensitivity dB/dP is given by the slope, which is 1.56×10^{-5} MPa^{-1} in the pressure range from 0.00 to 0.06 MPa with the presented load applying configuration. From the similar slopes observed in the low and high pressure ranges (Figure 5, right), the sensor is considered to have a fairly linear response to the pressure at 0.00−0.06 MPa.

Dynamic Range. Figure 6 shows the intensity change obtained when the pressure was continuously increased from 0.00 to 0.47 MPa. A theoretical curve that is calculated based on the obtained polarimetric sensitivity is superimposed on the measured points as a dotted line in Figure 6, for the purpose of showing the change in the sensor performance at higher pressure.

The output intensity is calculated based on Malus' law as shown in eq 5, with the input polarization tilted by θ_{pol} referring to the slow (x_1) and fast (x_2) axes and the projection components to the fast and slow axes $A \sin \theta_{pol}$ and $A \cos \theta_{pol}$, respectively, where A is the amplitude of the incident light wave. The amplitudes of the two components passing through the analyzer are $A \sin \theta_{pol} \sin \theta_A$ and $A \cos \theta_{pol} \cos \theta_A$. The phase shift δ between the x_1 and x_2 components is calculated from dB/dP, which is obtained as described previously. Both θ_{pol} and θ_A are 45°.

$$I_{Malus} = (A \cos \theta_{pol} \cos \theta_A)^2 + (A \sin \theta_{pol} \sin \theta_A)^2 + 2A^2 \cos \theta_{pol} \sin \theta_{pol} \cos \theta_A \sin \theta_A \cos \sigma \quad (5)$$

As a result, the intensity contrast decreased gradually with increasing pressure. A change in the polarimetric sensitivity is also observed, where the intensity oscillation pitch differs at higher pressure. The intensity oscillation decreases and becomes undetectable at a pressure above 0.45 MPa.

Additionally, a fitting curve that was obtained by modifying the last term of eq 5 was drawn in order to characterize

Table 2. Numerical Data of Applied Pressure P, Observed Power, Phase Shift δ, and Birefringence B[a]

P (MPa)	power (μW)	δ (rad)	B
3.27×10^{-3}	123.8	0.0662π	5.24×10^{-8}
8.17×10^{-3}	116.5	0.1627π	1.29×10^{-7}
1.63×10^{-2}	92.0	0.3236π	2.56×10^{-7}
2.86×10^{-2}	47.2	0.5650π	4.47×10^{-7}
4.41×10^{-2}	10.3	0.8836π	6.99×10^{-7}
4.82×10^{-2}	5.1	0.9511π	7.53×10^{-7}
5.23×10^{-2}	4.4	1.0316π	8.17×10^{-7}
5.39×10^{-2}	5.4	1.0637π	8.42×10^{-7}
5.55×10^{-2}	7.1	1.0959π	8.68×10^{-7}
5.64×10^{-2}	8.4	1.1120π	8.80×10^{-7}
5.72×10^{-2}	9.4	1.1281π	8.93×10^{-7}

[a] δ and B are values at $\lambda = 633.3$ nm.

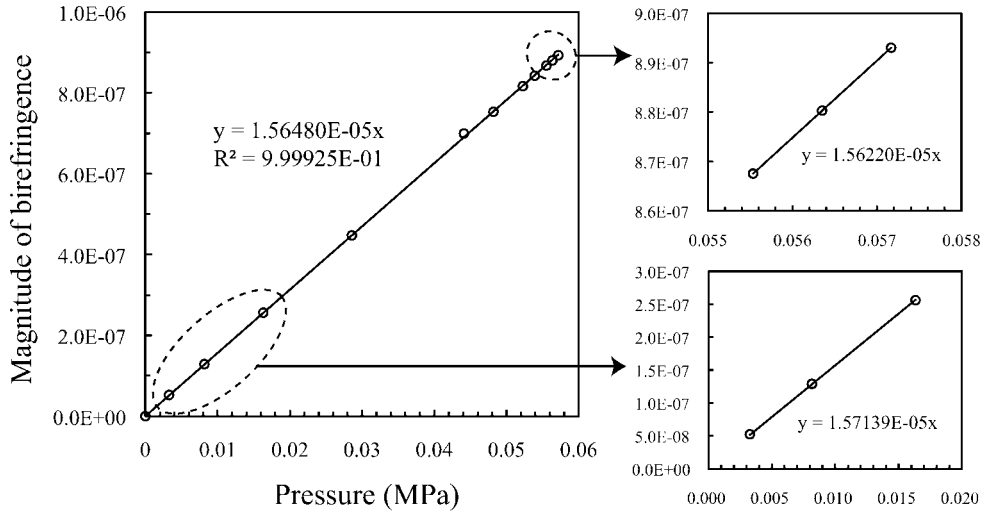

FIGURE 5. Birefringence shift upon pressure change plotted to estimate the polarimetric sensitivity. The obtained polarimetric sensitivity was 1.56 × 10^{-5} MPa^{-1}.

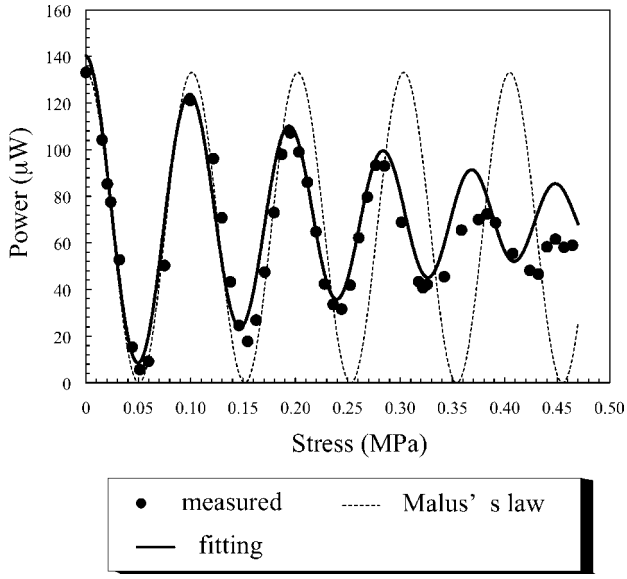

FIGURE 6. Intensity response to the applied pressure in the test range from 0.00 to 0.47 MPa when the pressure was continuously increased (plot). Theoretical curves based on Malus' law (broken line) and the fitting (solid line) are superimposed on the measured plots.

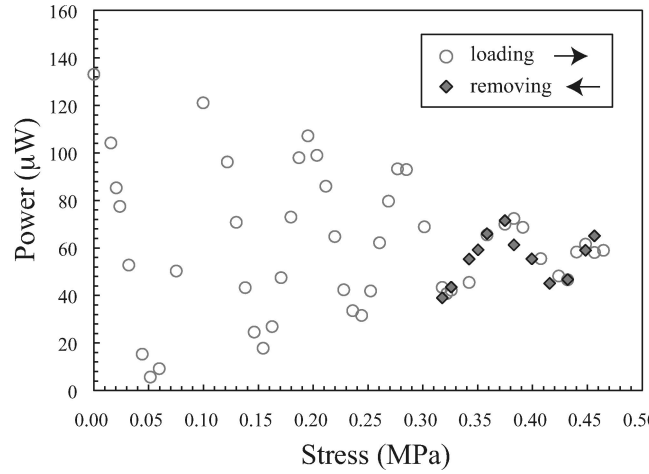

FIGURE 7. Power response to the applied pressure in the test range from 0.00 to 0.47 MPa. The open circle markers are identical with the data shown in Figure 6. The diamond markers represent the intensities observed when the load was continuously reduced.

the measured response (solid line in Figure 7). The fitting takes the form of eq 8. Both α and β in the equation are functions of the pressure P.

$$I_{fitting} = (A\cos\theta_{pol}\cos\theta_A)^2 + (A\sin\theta_{pol}\sin\theta_A)^2 + 2A^2\cos\theta_{pol}\sin\theta_{pol}\cos\theta_A\sin\theta_A\left(\frac{1}{e^{\alpha}}\cos(\varphi^{\beta})\right) \quad (6)$$

$$\alpha = \alpha(P) = P(2.5 + P^2) \quad (7)$$

$$\beta = \beta(P) = 1 + P^{0.08} \quad (8)$$

The terms $1/e^{\alpha}$ and β correspond to the decreasing contrast and the oscillation pitch, respectively. As a result, a fairly good match between the fitting and the measured curve is demonstrated.

Figure 7 shows the intensity changes when the pressure was gradually released after reaching a turning point at 0.47 MPa. The open circle markers are identical with the data shown in Figure 6. The diamond markers represent the intensities observed when the load was continuously reduced.

DISCUSSION

In Figure 4, a clear cosine curve is observed in the original configuration while the curves obtained from 0 and 90° configurations are practically flat. This result suggests that the fast and slow axes are clearly manifested in the phase retarder POF. In the case of 0 and 90° configurations, the linearly polarized input light does not split into ordinary and extraordinary components because the light vibrates in either parallel or perpendicular orientation to the optical axes.

At 0−0.06 MPa, a polarimetric sensitivity of 1.56 × 10^{-5} MPa^{-1} is obtained with a high correlation coefficient. This

suggests that the phase change in the phase retarder POF is stable enough to be detectable only by using a polarizer.

The effect of fiber deformation was investigated in order to understand the governing factors of the oscillation behavior in the 0−0.47 MPa pressure range. Equation 5 expresses the output intensity of a polarizer−analyzer system with a phase-shifting medium inserted. Because the phase shift is calculated using the measured dB/dP values with the assumption that eq 3 is satisfied, the curve takes a different shape if the proportionality between P and $\Delta\sigma$ is no longer given. Equation 3 can be applied only under conditions where (1) the fiber cross section is perfectly circular or deformed within 1% strain, (2) the top and bottom plates are positioned perpendicular to the fiber cross section, (3) the surfaces of the fiber and the plates are smooth, and (4) the guide center of the fiber is birefringence-free before stress application. Among the above requirements, (2) is considered to be satisfied with high precision because of the use of stabilizers. (3) is satisfied to a certain extent because both the fiber and the plates show highly reflecting surfaces. (4) is considered to be satisfied as well, judging from the refractive index profile that matches well on the zero-orientational line (Figure 1a).

To investigate the impact of (1), the extent of deformation was estimated by determining whether the fiber was deformed elastically or plastically at 0.47 MPa. Figure 7 shows the intensity change when the pressure was gradually released after reaching a turning point at 0.47 MPa.

The mechanical characteristics of PMMA are known to be hard and brittle at room temperature, and the stress−strain curve reaches a fracture point within 5% strain (25). The stress−strain relationship before the fracture point is close to linear, which can be considered as an elastic deformation. PMMA usually fractures before deforming plastically at a strain over 5%. The copolymer used for the phase retarder POF contains 82% PMMA, and thus the mechanical behavior of the test fiber is considered to be similar to that of a pure PMMA fiber. Hence, the original geometry of the fiber is considered to be restored if deformation is under 1% strain.

The pressure release trace observed in Figure 7 suggests that the fiber is not permanently deformed at 0.47 MPa pressure. Hence, the deformation of the fiber is considered to be below 1% strain in the performed measurements.

The terms α and β in the fitting (eq 8) express the contrast drop and inconsistency in the power oscillation pitch. Because the effect of deformation is suggested to be minor, these factors are considered to be the effect of multiple intermodal interference, in which the interference at over π retardation produces multiple states of polarization as an output because the slight phase variation among the modes becomes larger. Hence, multiple polarization states are considered to be coexisting in the output light at around 0.45 MPa pressure.

CONCLUSION

A phase retarder POF with a 667 μm core was fabricated using a birefringence-controllable copolymer, P(MMA/BzMA). The optimum composition that eliminates orientational birefringence, but still induces photoelastic birefringence, was suggested to be 82:18, based on the refractive index relationship. The periodic shift of ER values observed with a pressure increase illustrated a clear change in the polarization state of the phase retarder POF, whereas the other test fibers fabricated with different monomer compositions did not show such a property.

A simple sensor design with a single-fiber structure was proposed that has detection capabilities similar to those of the conventional dual-path structure of a Mach−Zehnder interferometer. The measured intensity showed a regular response to the pressure from 0 to 0.06 MPa. The polarimetric sensitivity obtained for that pressure range was 1.56×10^{-5} MPa^{-1}.

At higher pressure, the contrast and oscillation pattern of the intensity gradually decreased. This phenomenon was considered to be the effect of interference between multiple modes supported by the phase retarder POF.

REFERENCES AND NOTES

(1) Spillman, W. B., Jr. *Opt. Lett.* **1982**, *7*, 388.
(2) Graham, E. B.; Raab, R. E. *Proc. R. Soc. London, Ser. A* **1983**, *1798*, 73.
(3) Murray, R. T. *IEE Conf. Publ.* **1983**, *221*, 114.
(4) Rines, G. A. *Appl. Opt.* **1981**, *20*, 3453.
(5) Fields, J. N.; Asawa, C. K.; Ramer, O. G.; Barnoski, M. K. *J. Acoust. Soc. Am.* **1980**, *67*, 816.
(6) Pinet, E.; Cibula, E.; Donlagic, D. *Proc. SPIE* **2007**, *6770*, 67700U.
(7) Prohaska, J. D.; Snitzer, E.; Chen, B.; Maher, M. H.; Nawy, E. G.; Morey, W. W. *Proc. SPIE* **1993**, *1798*, 286.
(8) Kihara, M.; Ohno, H. *Trends Opt. Photonics* **2003**, *88*, 1918.
(9) Ohno, H.; Naruse, H.; Yasue, N.; Miyajima, Y.; Uchiyama, H.; Sakairi, Y.; Li, Z. X. *Proc. SPIE* **2001**, *4596*, 74.
(10) Bucaro, J. A.; Hickman, T. R. *Appl. Opt.* **1979**, *18*, 938.
(11) Bucaro, J. A.; Cole, J. H. *IEEE Electron. Aerospace Syst. Conv.* **1978**, *3*, 572.
(12) Shajenko, P.; Flatley, J. P.; Moffett, M. B. *J. Acoust. Soc. Am.* **1978**, *64*, 1286.
(13) Fields, J. N.; Asawa, C. K.; Smith, C. P.; Morrison, R. J. *Adv. Ceram.* **1981**, *2*, 529.
(14) Gahir, H. K.; Khana, D. *Appl. Opt.* **2007**, *46*, 1184.
(15) Lomer, M.; Quintela, A.; Quintela, M. A.; Cobo, A.; Lopez-Higuera, J. M. *Proc. SPIE* **2007**, *6619*, 661917.
(16) Muto, S.; Sato, H.; Hosaka, T. *Jpn. J. Appl. Phys.* **1994**, *33*, 6060.
(17) Bartlett, R. J.; Philip-Chandy, R.; Eldridge, P.; Merchant, D. F.; Morgan, R.; Scully, P. J. *Trans. Inst. Measure. Control* **2000**, *22*, 431.
(18) Liehr, S.; Lenke, P.; Krebber, K.; Seeger, M.; Thiele, E.; Metschies, H.; Gebreselassie, B.; Munich, J. C.; Stempniewski, L. *Proc. SPIE* **2008**, *7003*, 700302.
(19) Furukawa, R.; Tagaya, A.; Iwata, S.; Koike, Y. *J. Phys. Chem. C* **2008**, *112*, 7946.
(20) Furukawa, R.; Tagaya, A.; Iwata, S.; Koike, Y. *Jpn. J. Appl. Phys.* **2008**, *93*, 103303.
(21) Furukawa, R. A.; Tagaya, A.; Koike, Y. *Appl. Phys. Lett.* **2008**, *112*, 7946.
(22) Zubia, J.; Durana, G.; Arrue, J.; Garces, I.; Lopez-Amo, M. *Proc. SPIE* **2001**, *4595*, 213.
(23) Tagaya, A.; Ohkita, H.; Harada, T.; Ishibashi, K.; Koike, Y. *Macromolecules* **2006**, *39*, 3019.
(24) Ohtsuka, Y.; Koike, Y. *Appl. Opt.* **1980**, *19*, 2866.
(25) Carswell, T. S.; Nason, H. K. *Symposium on Plastics*; Philadelphia District Meeting; American Society for Testing Materials: West Conshohocken, PA, 1944.

AM800212Y